

TeV emission from SN 1006

A. Mastichiadis¹ and O.C. de Jager²

¹ MPI Kernphysik, Postfach 10 39 80, D-69029 Heidelberg, Germany

² Space Research Unit, PU vir CHO, Potchefstroom, South Africa

Received ; accepted

Abstract. Supernova 1006 is the first shell type supernova remnant to show evidence of particle acceleration to TeV energies. In the present paper we examine this possibility by modeling the observed X-ray non-thermal emission in terms of synchrotron radiation from Fermi accelerated electrons. The predicted synchrotron spectrum fits the radio and non-thermal component of the observed soft X-ray to hard X-ray emission quite well. These particles can produce TeV gamma rays by inverse Compton scattering on the microwave radiation and other ambient fields, and the derived electron distribution is also used to calculate the expected inverse Compton flux. We find that if the remnant is characterised by a magnetic field strength lower than $\sim 7\mu\text{G}$, then the TeV flux can be higher than that of the Crab Nebula. About 75% of the TeV emission from SN 1006 is expected to be concentrated in the synchrotron bright NE and SW rims (the “hard aegis”) of the remnant, which would allow a sensitive search if the Atmospheric Imaging Cherenkov Technique is used.

Key words: ISM: individual objects: SN1006 – ISM: magnetic fields – Gamma Rays: theory

1. Introduction

The type Ia supernova remnant G327.6+14.6, or SN 1006, is the remnant of the explosion which took place in AD 1006. The distance to this source is between 1.4 and 2.1 kpc (Green 1988). Its mean expansion rate has been measured as 0.44 ± 0.13 arcsec/yr, which implies a present expansion speed of 3700 ± 1300 km/s for an average distance of 1.8 kpc. The time dependence of the expansion ($R \propto t^{0.48 \pm 0.13}$) is consistent with Sedov expansion, or with a forward/reverse shock pair moving into constant-density material (Moffett, Goss, & Reynolds 1993).

The ASCA detection of power law X-ray emission from the bright northeastern (NE) and southwestern (SW) rims

of SN 1006 led Koyama et al. (1995) to infer the existence of electrons accelerated by the first order Fermi mechanism up to energies of ~ 200 TeV. The detection of TeV γ -rays from this system will prove the existence of such ultrarelativistic electrons (De Jager et al. 1995, Mastichiadis 1996, Pohl 1996).

In Section 2 we will compile the non-thermal radio to X-ray spectrum, which may be due to synchrotron emission from these electrons, and in Section 3 we will compare the acceleration and loss timescale for electrons accelerated by the first order Fermi process, and show that the resulting maximum electron energy predicts a synchrotron cutoff frequency which is consistent with observations. The best-fit spectrum also leads to the derivation of the magnetic field strength B_* associated with the shell. In Section 4 we will calculate the inverse Compton (IC) γ -ray spectrum associated with this best-fit model spectrum from Section 3. The detection of TeV γ -rays from SN 1006 will enable the observer to determine the magnetic field strength, and an important parameter associated with Fermi acceleration from the observed γ -ray flux.

2. The observed synchrotron spectrum of SN 1006

The radio morphology shows two bright arcs towards the NE and SW (see e.g. Reynolds & Gilmore 1993), with a composite spectrum which is given by

$$F_\nu = 16 \left(\frac{\nu}{10^9 \text{ Hz}} \right)^{-0.56} \text{ Jy}, \quad (1)$$

and shown in Fig. 1. The individual radio flux measurements for the total emission from SN 1006 (reproduced from Fig. 1 of Reynolds 1996) are also shown for comparison.

ROSAT imaging observations of SN 1006 shows that the soft X-ray remnant is dominated by thermal ($kT = 0.15$ keV) emission towards the SE, whereas the X-ray counterparts of the NE and SW radio rims (or “hard aegis”) are characterized by a power law spectrum which dominates the total emission from the remnant above ~ 1 keV (Willingale et al. 1996). Spatially resolved spectral

Send offprint requests to: O.C. de Jager

results by ASCA have shown that these bright rims are responsible for $\sim 75\%$ of the total X-ray flux from SN 1006 above 1 keV, and the interior of the remnant also contains this non-thermal emission, which dominates the thermal component above 2 keV (Koyama et al. 1995). The results from earlier non-imaging instruments are therefore useful to obtain the non-thermal spectrum above 1 keV from the entire remnant. For example: TENMA (Koyama et al. 1987), EXOSAT (Jones & Pye 1989), and Ginga (Ozaki et al. 1994) obtained well-constrained spectral energy indices ranging between -2.0 and -2.3 for energies between 1.5 keV and ~ 10 keV. This is confirmed by the energy index of -2.0 ± 0.2 of the NE rim found by ASCA (Koyama et al. 1995). The EXOSAT ME field of view was just large enough to cover the entire remnant, without significant background contamination, and the energy spectrum above 1.5 keV (derived from the given energy flux) is given by

$$F_\epsilon = 0.066 \epsilon_{\text{keV}}^{-2.0} \text{ keV.cm}^{-2} \text{s}^{-1} \text{keV}^{-1}, \quad (2)$$

which is shown together with the radio spectrum in Fig. 1.

The change from a -0.56 radio energy index to a ~ -2 X-ray energy index above ~ 1 keV is indicative of a spectral turnover or break around $\epsilon_b \sim 0.25$ keV, where the spectral energy index should be around -1 (depending on the sharpness of the cutoff). In fact, soft X-ray imaging observations of the hard aegis by the EINSTEIN SSS (Becker et al. 1980) and EXOSAT LE (Jones & Pye 1989) resulted in a consistent spectral energy index of -1.2 . Willingale et al. (1996) used ROSAT PSPC observations to separate the thermal and non-thermal energy fluxes of the hard aegis and the rest of the remnant, with the same finding as Koyama et al. (1995) that the non-thermal soft X-ray flux from the hard aegis contributes to $\sim 75\%$ of the total non-thermal soft X-ray flux of 2.66×10^{-10} ergs/cm²/s (for the 0.1 keV to ~ 2 keV range). Assuming the average spectral index of -1.2 found by EINSTEIN and EXOSAT (Willingale et al. 1996 obtained a spectral index for the SW limb only), but using the ROSAT normalization for the total non-thermal flux from SN 1006, the resulting energy spectrum for this energy range is therefore

$$F_\epsilon \sim 0.047 \epsilon_{\text{keV}}^{-1.2} \text{ keV.cm}^{-2} \text{s}^{-1} \text{keV}^{-1}, \quad (3)$$

and is indicated by its spectral index in Fig. 1.

3. First order Fermi acceleration of electrons in SN 1006

The non-thermal synchrotron emission of SN1006 from shock accelerated electrons has been discussed by Reynolds & Chevalier (1981), Ammosov et al. (1994) and, more recently, by Reynolds (1996). Here we apply the method given in Mastichiadis (1996 - henceforth M96). This allows us to treat the problem in a self-consistent

manner by calculating the electron distribution function at each instant in time from the solution of a time-dependent kinetic equation for electrons. The physical picture is according to the ‘Onion-shell-model’ (Bogdan & Völk 1983) as applied to time-dependent acceleration (Ball & Kirk 1992). Therefore we assume that electrons are accelerated in the (parallel) shock wave of the expanding supernova remnant and at each instance there is a flux of relativistic electrons which escape downstream and subsequently radiate. For these we assume to have a power law spectrum in energy, i.e. $Q_e(E, t) = Q_{e,0}(t)E^{-s}$ with $E \leq E_{\text{max}}(t)$ and an exponential cut-off for $E > E_{\text{max}}(t)$ (Webb et al. 1984). For the determination of the normalization factor we followed M96 (after an original suggestion by Drury 1992) and set $Q_{e,0}(t) \propto R(t)^2 u_{\text{sh}}(t)^3$ where $R(t)$ is the radius of the supernova and $u_{\text{sh}}(t)$ is the velocity of the shock. Furthermore, the maximum energy electrons can achieve at a time t depends on whether synchrotron losses become dominant or not and it is given by the minimum of (Lagage & Cessarsky 1983, Webb et al. 1984, M96 and Reynolds 1996)

$$E_{\text{acc}}(t) \simeq 5.10^{-3} A(r_c) f^{-1} u_{\text{sh}}(t)^2 B t_{\text{yr}} \text{ erg} \quad (4)$$

and

$$E_{\text{loss}}(t) \simeq 2.10^{-4} f^{-1/2} A(r_c)^{1/2} u_{\text{sh}}(t) B^{-1/2} \text{ erg}, \quad (5)$$

where u_{sh} is the shock velocity in units of km/sec, B is the magnetic field strength in Gauss, t_{yr} is the supernova remnant age in years, and $A(r_c) = (r_c - 1)/r_c(r_c + 1)$ with r_c being the compression ratio of the shock connected with the spectral index s through the relation $s = (r_c + 2)/(r_c - 1)$. Also f is the gyrofactor, i.e. the ratio of the particle’s mean free path to its gyroradius. The case $f = 1$ corresponds to a simple Bohm diffusion.

The relevant energy losses which were included in the kinetic equation were adiabatic due to the expansion of the remnant, synchrotron and inverse Compton. The only free parameter here is the magnetic field as the photon fields on which the electrons lose energy by inverse Compton scattering are rather well determined (see section 4 below).

Adopting standard supernova parameters, i.e. a total explosion energy of $W_{\text{SN}} = 5.10^{50} W_{5,50}$ erg, an initial shock velocity of $u_{\text{sh},\text{in}} = 7.10^3 u_{7,3}$ km/sec and an external matter density of $\rho = 0.4 \rho_{0.4}$ H-atom/cm³ (Willingale et al. 1996) we solved numerically the electron kinetic equation which includes a source term and loss terms as these were described above (for more details see M96). The obtained electron distribution function was folded with the synchrotron emissivity to obtain the radiated spectrum as this should be observed at a time $t_{\text{now}} \simeq 1,000$ years. This way we have made numerical fits to the radio/X-ray data by treating as free parameters the strength of the magnetic field downstream, the gyrofactor f and the shock compression ratio r_c .

Fig.1 shows the best fit to the radio and X-ray spectra (shown here as full lines) which was obtained for $B = 3.5f^{2/3} \mu\text{G}$ and $r_c = 3.73$ (corresponding to $s = 2.1$). This fit holds for $f \lesssim 30$. As f increases above this value the spectrum starts to break due to synchrotron losses and no satisfactory fit could be found. Therefore X-ray data alone might not be able to constrain f significantly. More constraints on f can be placed from future TeV observations as we will show in the next section.

We proceed now by giving a simple qualitative picture which will help in the understanding of our results: According to the standard picture of cosmic ray acceleration in supernova remnants (see, for example, Dorfi 1991) both $Q_{e,0}$ and E_{acc} peak close to the transition of the supernova remnant from its free expansion to its Sedov phase which occurs at $t_{\text{Sd}} \simeq 410W_{5,50}^{1/3}\rho_{0.4}^{-1/3}u_{7,3}^{-5/3}$ yr. For example, $E_{\text{acc}} \propto t$ for $t < t_{\text{Sd}}$ and $E_{\text{acc}} \propto t^{-1/5}$ for $t > t_{\text{Sd}}$. Similarly, $Q_{e,0} \propto t^2$ for $t < t_{\text{Sd}}$ and $Q_{e,0} \propto t^{-1}$ for $t > t_{\text{Sd}}$. Therefore the radiation observed now should be dominated by the particles accelerated at $t \gtrsim t_{\text{Sd}}$. Using Eqn. (4) we get that the maximum particle energy at $t \simeq t_{\text{Sd}}$ is given by

$$E_{\text{acc,Sd}} \simeq 1.5 \cdot 10^7 B f^{-1} g^{-1} W_{5,50}^{1/3} \rho_{0.4}^{-1/3} u_{7,3}^{1/3} \text{ erg.} \quad (6)$$

g is a factor (of order unity) that reflects the fact that at $t = t_{\text{Sd}}$ the velocity is not any more $u_{\text{sh,in}}$ but somewhat smaller since deceleration of the shock should have started before that time. This in turn implies that the energy E_{acc} as given by Eqn. (6) is, strictly speaking, an upper limit of the maximum energy the electrons can attain during acceleration.

Equation (6) is the maximum energy electrons can attain as long as this is smaller than E_{loss} (equation [5]). A comparison of the two expressions for $t = t_{\text{Sd}}$ yields that this is indeed the case as long as $B \lesssim 10^{-5} f^{1/3} g^{1/3} W_{5,50}^{2/9} \rho_{0.4}^{-2/9} u_{3,7}^{4/9}$ G. If this relation is satisfied then synchrotron losses do not become important at any epoch, since for $t > t_{\text{Sd}}$, $E_{\text{acc}} \propto t^{-1/5}$ while $E_{\text{loss}} \propto t^{-3/5}$.

From the above discussion it becomes evident that if radiation losses do not become important then the synchrotron spectrum that the current model predicts can be fairly well represented by the synchrotron spectrum which is derived from a simple electron distribution function (power law times exponential cutoff) of the form

$$\frac{dN}{dE} \simeq 1.5 \times 10^3 \left(\frac{B}{B_*}\right)^{-1.56} E^{-2.12} \exp\left[-\frac{E}{E_b} \left(\frac{B}{B_*}\right)^{1/2}\right] 4\pi d^2, \quad (7)$$

with units in total number of electrons per erg while E is in ergs. The best-fit value for the magnetic field is given by $B_* = 3.5f^{2/3}g^{2/3}W_{5,50}^{-2/9}\rho_{0.4}^{-2/9}u_{7,3}^{2/3} \mu\text{G}$ while $E_b = E_{\text{acc,Sd}}$. The area factor $4\pi d^2$ allows us to calculate photon spectra in terms of the flux at Earth if $(dN/dE)/4\pi d^2$ is used. Using the best fit value for B_* the total energy content in relativistic electrons is $\simeq 10^{49} f^{-1.04} g^{-1.04} W_{5,50}^{0.35} \rho_{0.4}^{-0.35} u_{7,3}^{0.35}$

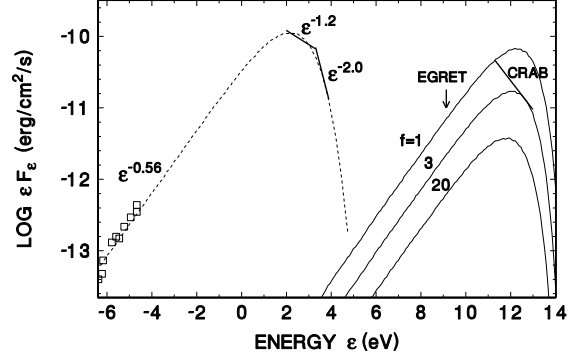


Fig. 1. Plot of the best fit synchrotron spectrum (thin dashed line) and inverse Compton spectra (thin solid lines indicated by the f -values as described in Section 3) calculated from the time-dependent electron continuity equation (Section 3). The open squares are the radio flux measurements reproduced from Reynolds (1996). The thick solid lines represent the observed X-ray spectra corresponding to Eqns. (2), and (3) as discussed in Section 2, and indicated by their spectral indices. The thick dashed line is the Crab spectrum given by Djannati-Ataï (1995).

erg. This in turn gives us an efficiency of cosmic ray electron production of

$$\eta_{\text{el}} \simeq 0.02 f^{-1.04} g^{-1.04} W_{5,50}^{-0.65} \rho_{0.4}^{-0.35} u_{7,3}^{0.35} \quad (8)$$

in rough agreement with the hypothesis that about a few percent of the supernova energy available for acceleration goes to electrons.

4. The expected γ -ray spectrum of SN 1006

Several soft photon fields may contribute to the inverse Compton (IC) scattering of relativistic electrons into the γ -ray region. De Jager (1996) discussed the production of γ -ray spectral features introduced by the scattering of several thermal photon spectra by the electron cutoff (with maximum electron energy $\gamma_b mc^2$) in SNR W44, which may explain the EGRET detection (2EG J1857+0118, Thompson et al. 1996) of this remnant. The cutoff in the spectrum derived in Section 3 will similarly produce γ -ray bumps on a ϵF_ϵ plot (as in Fig. 1) at γ -ray energies $\sim 3kT_i \gamma_b^2$ (in the Thomson limit) or $\sim \gamma_b mc^2$ (in the Klein-Nishina limit), with $T_1 = 2.76\text{K}$ representing the CMBR, $T_2 \sim 25\text{K}$ the galactic dust contribution, $T_3 = 3,000 - 4,000\text{K}$ representing the Population II stars, and $T_4 \sim 7,500\text{K}$ representing the contribution from Population I stars, with densities given by Skibo (1993). Arendt (1989) also did not detect any significant FIR emission associated with swept up dust in SN 1006, so that there would be no contribution to soft photons from sources inside or near SN 1006,

in contrast with W44 where the emission from swept-up dust dominates all soft photon fields.

We include all soft photon fields, using the full cross section for isotropic IC as reviewed by Blumenthal & Gould (1970) in the calculation of the γ -ray spectrum. The IC spectra calculated from the best-fit electron spectrum (Eqn. [7]) for different f -values are also shown in Fig. 1, and it is clear that the γ -ray energy flux peaks at a few TeV (nearly independent of the value of f), the dominant source of this bump being the CMBR photons scattered in the Thomson limit. The integral flux above 1 TeV is given by

$$F(> 1\text{TeV}) = 4.1 \times 10^{-11} f^{-1.35} \text{ cm}^{-2}\text{s}^{-1}, \quad (9)$$

with f constrained to values below ~ 20 . The Crab spectrum in the range 0.5 to 10 TeV (Djannati-Ataï 1995) is also shown for comparison in Fig. 1, and it is clear that we may expect SN 1006 to be a stronger source than the Crab at 1 TeV if $f < 3$. It is also clear that the EGRET upper limit of SN 1006 shown in Fig. 1 does not constrain f significantly, but TeV observations will provide valuable limits.

Finally we would like to note that the TeV flux as given above is about an order of magnitude higher than the expected flux from the nuclear component of cosmic rays assumed to be accelerated also at the supernova shock (Drury et al. 1994).

5. Summary-Discussion

The recent X-ray observations of SN 1006 (Koyama et al. 1995) make a strong case for particle acceleration in supernova remnants. A necessary consequence of this is that SN 1006 can be a source of TeV radiation as the accelerated electrons will scatter off the ambient soft photons to very high energies. In the present paper we calculated the expected TeV flux by following the basic principles of first order Fermi shock acceleration to fit the radio/X-ray observations and consequently we used the derived electron distribution function to calculate the TeV emissivity. In this case we found that the TeV flux depends sensitively on the gyrofactor f of the accelerated electrons and consequently one can use any future TeV observations of SN 1006 to put limits on this.

We find that the EGRET upper limit (derived from Thompson et al. 1996) does not constrain f significantly, but imaging TeV observations have no difficulties observing sources nearly 10 times weaker than the Crab. We may therefore be able to detect SN 1006 at TeV energies if f is not too large. The NE and SW limbs may be detectable by the Atmospheric Imaging Cherenkov Technique (see e.g. Weekes et al. 1989) if a search for the NE and SW rims are made. However, the flux for each rim would be $\sim 38\%$ of the flux given in Eqn. (9) for the total TeV emission from SN 1006, but by superimposing the pixels from the TeV

image corresponding to the NE and SW rims, the total flux should be about 75% of the flux given in Eqn. (9).

Acknowledgements. AM would like to thank the Deutsche Forschungsgemeinschaft for support under Sonderforschungsbereich 328 and the staff and members of the Space Research Unit of the Potchefstroom University for their hospitality.

References

- Ammosov, A.E., et al., 1994, *Astr.Lett.* 20, 191
 Arendt, R.G., 1989, *ApJS* 70, 181
 Ball, L.T. & Kirk, J.G., 1992, *ApJLett* 396, L39
 Becker, R.H., et al., 1980, *ApJ* 240, L33
 Blumenthal, G.R. & Gould, R.J.: 1970, *Rev. Mod. Physics* 42(2), 237
 Bogdan, T.J., Völk, H.J., 1983, *A&A* 122, 129
 De Jager, O.C., et al., 1995, 24th ICRC 1, 528
 De Jager, O.C., 1996, in *Cold dust morphology in galaxies*, ed. D. Block, Kluwer Academic Publ. (Dordrecht, Holland), in press
 Djannati-Ataï A., et al., 1995, in: *Proc. 24th ICRC (Rome)*, Vol. 2, p.315
 Dorfi E.A., 1991, *A&A* 251, 597
 Drury, L.O'C., 1992, in *Particle Acceleration in Astrophysics*, eds. G.P. Zank, T.K. Gaisser, AIP, New York, 189
 Drury L.O'C., Aharonian A.F., Völk H.J., 1994, *A&A* 287, 959
 Green, D.A. 1988, *Astrophysics & Space Science* 148, 3
 Jones, L.R., & Pye, J.P., 1989, *MNRAS* 238, 567
 Koyama K., Tsunemi, H., Becker, R.H., & Hughes, J.P. 1987, *PASJ* 39, 437
 Koyama K., et al. 1995, *Nature* 378, 255
 Lagage P.O., Cesarsky C.J., 1983, *A&A* 125, 249
 Mastichiadis, A. 1996, *A&A* 305, L53–M96
 Moffett, D.A., Goss, W.M., & Reynolds, S.P. 1993, *AJ* 106, 1566
 Ozaki, M., Koyama, K., Ueno, S., & Yamauchi, S., 1994, *PASJ* 46, 367
 Pohl, M., 1996, *A&A* 307, 57
 Reynolds, S.P., Chevalier R.A., 1981, *ApJ* 245, 912
 Reynolds, S.P., & Gilmore, D.M., 1993, *AJ* 106, 272
 Reynolds, S.P., 1996, *ApJ* 459, L13
 Skibo J.G., 1993, Ph.D. thesis, Univ. of Maryland
 Thompson, D.J., et al. 1996, *ApJS*, in press
 Webb G.M., Drury L.O'C., Biermann P., 1984, *A&A* 137, 185
 Weekes, T.C., et al., 1989, *ApJ* 342, 379
 Willingale, R., West, R.G., Pye, J.P., & Stewart, G.C. 1996, *MNRAS* 278, 749.